Heliyon

ELSEVIER

Received:
28 August 2018
Revised:
13 October 2018
Accepted:
12 November 2018

Cite as: Xiangming Li, Rui Li, Guojian Yuan, Mengyao Zheng, Zhen Meng, Jia Guo, Guangyou Zhou. Fabrication and microstructure of quartz ceramics with orderly−arranged carbon filler. Heliyon 4 (2018) e00935. doi: 10.1016/j.heliyon.2018.e00935

Fabrication and microstructure of quartz ceramics with orderly−arranged carbon filler

Xiangming Li*, Rui Li, Guojian Yuan, Mengyao Zheng, Zhen Meng, Jia Guo, Guangyou Zhou

School of Environment and Materials Engineering, Yantai University, Yantai, Shandong, 264005, PR China

* Corresponding author.

E-mail address: li_xiangming@yahoo.com (X. Li).

Abstract

Ceramics with tailored pore structure are showing potential applications in some special fields. For fabricating quartz ceramics with orderly−arranged carbon filler, a combination of 3D printing, vacuum suction filtration and sintering was explored to fabricate quartz ceramics with highly−ordered and well−connected big pore channels. The spatial lattice structure in the polylactic acid (PLA) template fabricated by 3D printing together with raw material ratio and sintering temperature has great effect on the properties and pore structure of the porous quartz ceramics. To demonstrate the technical feasibility for fabricating quartz ceramics with orderly−arranged filler, carbon powder was taken as an example and fully filled in the big pore channels of the porous quartz ceramics via vacuum impregnation method. By choosing the quartz ceramics with only highly−ordered and well−connected big pore channels as substrate, quartz ceramics with orderly−arranged carbon filler were successfully obtained.

Keyword: Materials science

https://doi.org/10.1016/j.heliyon.2018.e00935

1. Introduction

Porous ceramics have attracted increasing attention and been widely used in many fields, such as separation materials [1, 2], catalyst supports [3, 4], bone substitute [5, 6], etc. Cold−pressing followed by sintering is a common method to fabricate porous ceramics with simple shape [7, 8, 9, 10]. Besides, some advanced techniques such as gelcasting [11, 12, 13, 14], freeze casting [15, 16, 17, 18] and direct forming [19] have been newly explored for fabricating porous ceramics. Basically, the porous ceramics fabricated by these methods have good structural and functional properties due to their uniform microstructure and well−distributed pores.

Recently, ceramics with tailored pore structure have been showing potential applications in some special fields. In the field of bone tissue engineering, bioscaffolds should have a certain amount of well−connected big pore channels with diameter in the range of 200−500 μm for the transport of body fluids and cells such as osteoclasts and osteoblasts [20]. Besides, bioscaffolds should also contain uniform−distributed small pores with diameter of 2−5 μm for facilitating the attachment of cells and the excretion of metabolic waste [21, 22, 23]. In the field of electromagnetic absorption, orderly arranging carbon filler in materials with low−permittivity is an effective method to improve the electromagnetic absorbing property of the carbon−containing materials. For example, electromagnetic wave could enter epoxy resin material with little reflection and then be attenuated by the orderly−arranged carbon fibers in the epoxy resin material [24, 25]. Similarly, if carbon filler is orderly−arranged in the ceramics with low−permittivity, the carbon−containing ceramics could also possess good electromagnetic absorbing property. Furthermore, these carbon−containing ceramics could be used in harsh environment for long time because of their excellent chemical and environmental stability.

To obtain ceramics with orderly−arranged carbon filler, the ceramics with highly−ordered and well−connected big pore channels should be fabricated firstly. This paper demonstrates an effective means to fabricate ceramics with tailored pore structure and those with orderly−arranged carbon filler. Due to the low permittivity of quartz, a combination of 3D printing, vacuum suction filtration and sintering is explored to fabricate quartz ceramics with highly−ordered and well−connected big pore channels. The effect of raw material ratio and sintering temperature on the shrinkage, open porosity, compression strength and microstructure of the porous quartz ceramics is studied. Additionally, in order to show the technical feasibility of introducing carbon filler in the quartz ceramics, the microstructure of quartz ceramics with orderly−arranged carbon filler fabricated via vacuum impregnation process is demonstrated.

https://doi.org/10.1016/j.heliyon.2018.e00935

2. Experimental

Calcium carbonate powder ($CaCO_3$) was mixed with talc powder ($Mg_3[Si_4O_{10}](OH)_2$) at a weight ratio of 1:1. The obtained mixture was used as additive and added in quartz powder containing 5 wt% of albite ($NaAlSi_3O_8$) and 5 wt % of microcline ($KAlSi_3O_8$) at levels of 10, 20 and 30 wt% respectively. The new obtained mixture was ball−milled in the planetary ball grinder for 2 h at a high speed (rotation speed of 360 r/min, revolution speed of 400 r/min), and ball−milled again for 10 min into slurry by adding ethanol. The weight content of ethanol in the slurry was controlled at about 25 wt%.

The PLA template with spatial lattice structure is printed out by a 3D printer (CR−10, Shenzhen Creality 3D Technology Co. Ltd, China). Fig. 1 shows one layer sliced from the PLA template. As can be seen, the spatial lattice structure in the template is formed by orderly−arranging circular columns in X, Y and Z directions. The inner diameter and height of the template is 20 and 36 mm respectively. The diameter of the columns is 0.6 mm, and the center distance between every two adjacent columns is 2.0 mm.

Fig. 2 schematic shows the fabrication process of quartz ceramics with orderly−arranged carbon filler. Firstly, assembled the template with filter paper and base, vacuumized the air in the base by a vaccum pump and added slurry slowly into the template. As the template was fully filled with powder blend, stop adding slurry and continued vacuumizing for 2 h. During the vacuumizing process, the ethanol in the slurry in the template was removed completely. Secondly, put the template containing powder blend in a furnace and sintered it at 1150−1250 °C for 2 h in air. During the sintering process, after removing the template because of oxidation, quartz ceramics with highly−ordered and well−connected big pore channels were

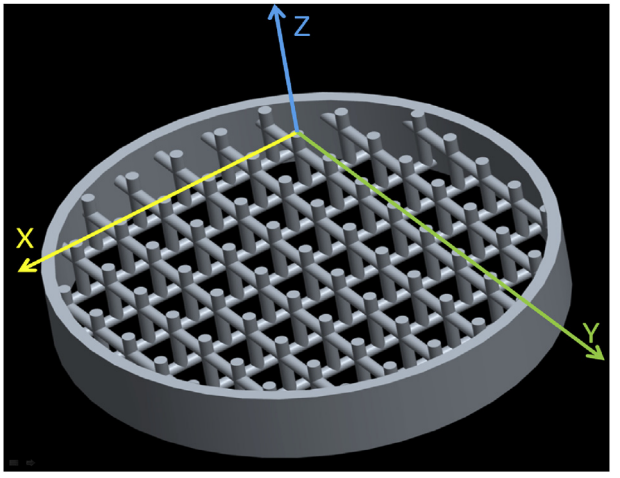

Fig. 1. One layer sliced from the PLA template with spatial lattice structure.

https://doi.org/10.1016/j.heliyon.2018.e00935

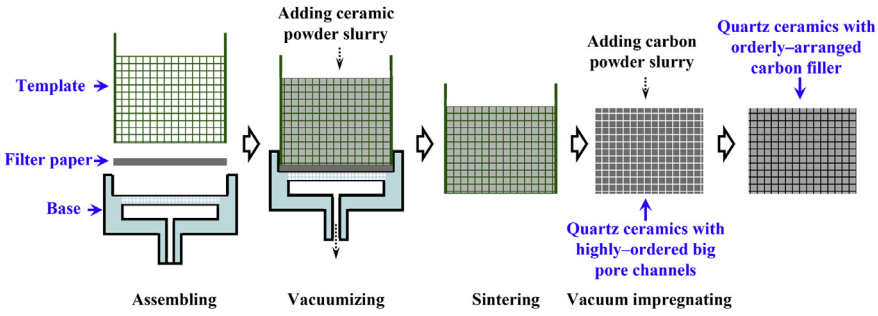

Fig. 2. Schematic of the fabrication process of quartz ceramics with orderly−arranged carbon filler.

obtained. Finally, dipped the porous quartz ceramics in slurry comprising carbon powder (analytical pure, 1000 mesh), polyvinyl alcohol and distilled water at a weight ratio of 75:1:24. When the big pores in the porous quartz ceramics were fully filled with carbon powder via vacuum impregnation method, quartz ceramics with orderly−arranged carbon filler were obtained by drying at 60 °C for 10 h.

The phase analyses were conducted by X−ray diffraction (XRD, XRD−7000, Shimadzu, Japan). Microstructure was observed by scanning electron microscopy (SEM, JSM−7610F, JEOL, Japan). Before SEM observation, all samples were polished with 0.5 μm diamond paste as a final polishing step. Shrinkage was estimated by measuring the center distance between the big pore channels of the porous quartz ceramics. Open porosity was measured by Archimedes method. Five cylindrical samples of 30 × 15 mm^2 diameter were tested to obtain the average compression strength via uniaxial compression test. Pore size distribution was measured using a Mercury Porosimeter (Poremaster 33, Quantan, USA). To facilitate the following discussion, the porous quartz ceramic fabricated from the powder blend with *m* wt% of additive at temperature of *n* °C is denoted as PQ−*m*−*n* (*m* is 10, 20 or 30, *n* is 1150, 1200 or 1250), and the corresponding quartz ceramic with carbon filler is named as PQ−*m*−*n*−C.

3. Results and discussion

Table 1 shows the properties of the porous quartz ceramics. Albite and microcline could decrease effectively the melting temperature of quartz, so the quartz in the powder blend is in molten state when sintering at 1150−1250 °C with the help of albite and microcline [26, 27], and the increase of fluidity of molten quartz with temperature rising will promote the shrinkage of the porous quartz ceramics. As shown in Table 1, the volume shrinkage of PQ−(10, 20 and 30) increases rapidly from 21.6%, 17.2% and 15.1%−34.1%, 29.0% and 32.3% respectively as the temperature rises from 1150 to 1200 °C, and then increases slowly to 33.7%, 30.7% and 33.0% respectively with temperature rising from 1200 to 1250 °C. The addition of talc has restraining effect on the shrinkage of ceramics [28, 29, 30], so basically the volume

https://doi.org/10.1016/j.heliyon.2018.e00935

Table 1. Properties of the porous quartz ceramics.

Sample number		Volume shrinkage (%)	Open porosity (%)	Compression strength (MPa)
SO−10	−1150	21.6	27.2	8.5
	−1200	34.1	18.2	44.2
	−1250	33.7	7.2	61.9
SO−20	−1150	17.2	34.8	6.4
	−1200	29.0	23.3	39.4
	−1250	30.7	9.9	46.6
SO−30	−1150	15.1	39.4	4.1
	−1200	32.3	28.6	34.6
	−1250	33.0	16.7	38.4

shrinkage of the porous quartz ceramics decreases gradually with the increase of talc in powder blend. As shown in Table 1, the volume shrinkage of PQ−(1150, 1200 and 1250) decreases respectively from 21.6%, 34.1% and 33.7%−17.2%, 29.0% and 30.7% as the additive in powder blend increases from 10 to 20 wt%. As the talc in powder blend increases further, the more silica deriving from the decomposition of talc will promote the shrinkage of porous quartz ceramics especially at higher temperature. Therefore, as the additive in powder blend increases from 20 to 30 wt%, the volume shrinkage of PQ−1150 decreases from 17.2% to 15.1%, while the volume shrinkage of PQ−(1200 and 1250) increases respectively from 29.0% and 30.7%−32.3% and 33.0%.

Fig. 3 shows the XRD patterns of PQ−(10, 20 and 30). As can be seen, PQ−(10, 20 and 30) are composed of a primary phase of quartz and a secondary phase of diopside ($CaMgSi_2O_6$) and cristobalite no matter what the sintering temperature is. As the additive in powder blend increases, the peak height of quartz decreases slowly with the peak height of diopside increasing gradually. As the temperature rises from 1150 to 1250 °C, the peaks of diopside become clearer and sharper, the peak height of cristobalite increases, and the amount of amorphous silica increases gradually. Diopside has much higher strength than quartz, so the increase of calcium carbonate in powder blend is theoretically conducive to improving the strength of the quartz ceramics. However, for porous ceramics, the increase of shrinkage will lead to decrease in porosity, and the decrease of porosity generally gives rise to an increase in compression strength. As shown in Table 1, as the temperature rises from 1150 to 1250 °C, PQ−(10, 20 and 30) decrease respectively in open porosity from 27.2%, 34.8% and 39.4%−7.2%, 9.9% and 16.7% due to the increase of shrinkage. During sintering, besides the restraining effect of talc on shrinkage, the decomposition of more calcium carbonate will increase the porosity of quartz ceramics, so PQ−(1150, 1200 and 1250) increase respectively in open porosity from 27.2%, 18.2% and 7.2%−39.4%, 28.6% and 16.7% as the additive in powder blend increases from 10 to 30 wt%. Due to the decrease of porosity with temperature rising from 1150 to 1250 °C, PQ−(10, 20 and 30) increases rapidly in compression strength

https://doi.org/10.1016/j.heliyon.2018.e00935

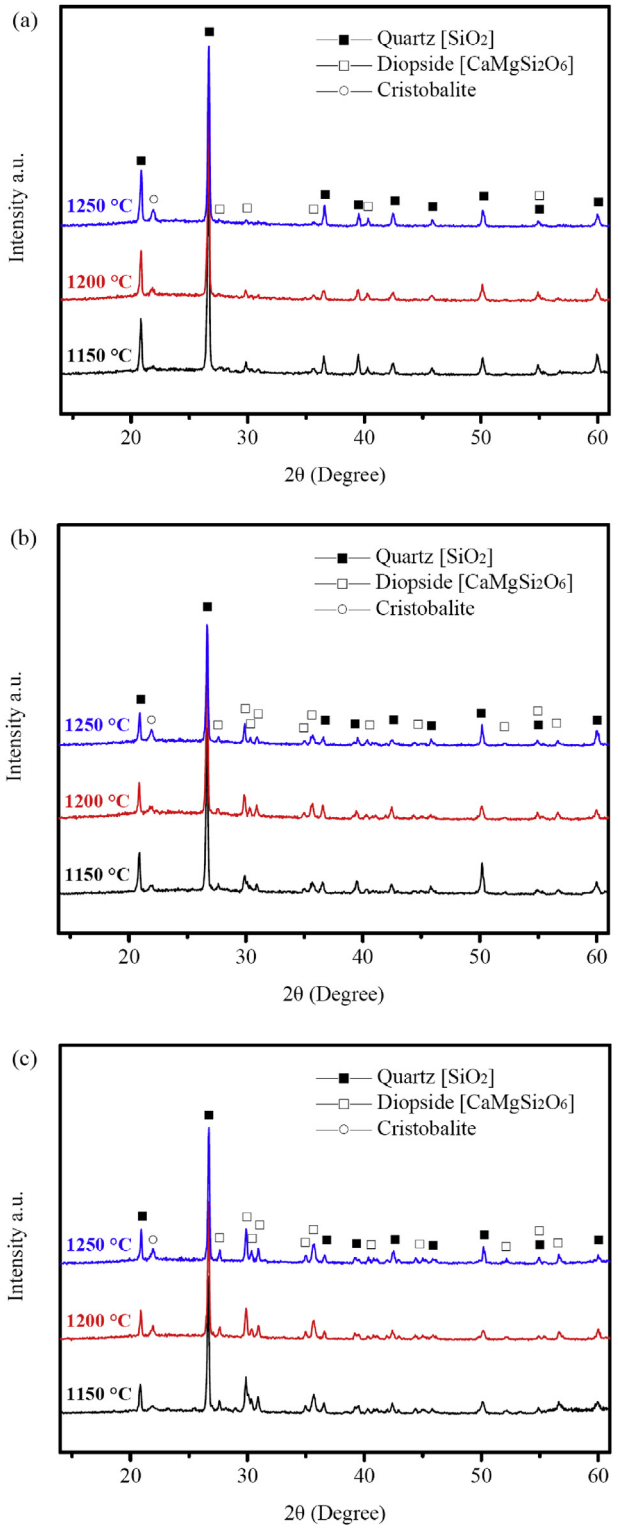

Fig. 3. XRD patterns of (a) PQ−10, (b) PQ−20 and (c) PQ−30.

https://doi.org/10.1016/j.heliyon.2018.e00935

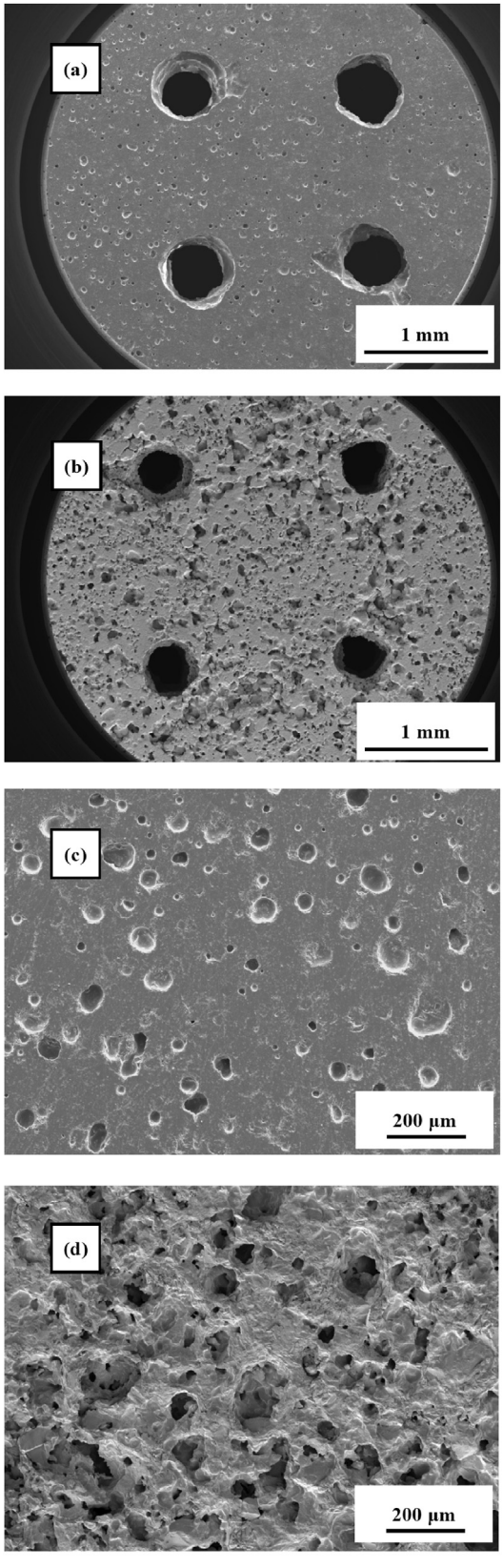

Fig. 4. SEM micrographs of PQ−10−1200 ((a) low magnification and (c) high magnification) and PQ−30−1200 ((b) low magnification and (d) high magnification).

https://doi.org/10.1016/j.heliyon.2018.e00935

from 8.5, 6.4 and 4.1 MPa to 61.9, 46.6 and 38.4 MPa respectively. Because of the increase of porosity as the additive in powder blend increases from 10 to 30 wt%, PQ−(1150, 1200 and 1250) decrease gradually in compression strength from 8.5, 44.2 and 61.9 MPa to 4.1, 34.6 and 38.4 MPa respectively.

Based on the results in Table 1, PQ−(10, 20 and 30)−1200 have sufficient compression strength and relatively high open porosity. Fig. 4 shows the SEM micrographs of PQ−(10 and 30)−1200 after polishing. From the low magnification micrographs in Fig. 4(a−b), the microstructures of PQ−(10 and 30)−1200 are uniform without defect, the big pore channels faithfully replicating the spatial lattice structure in the template (Fig. 1) are orderly distributed, the wall of big pore channels is smooth with hardly any defect and sharp angle. From the micrographs (Fig. 4(c−d)) taken from the matrix among the big pore channels, the microstructures of PQ−(10 and 30)−1200 are much different with each other. The sporadically distributed small pores in PQ−10−1200 are independent of each other, while a large number of small pores in PQ−30−1200 are uniformly−distributed and well−connected with each other.

Fig. 5 shows the volume percentage of the pores in PQ−(10 and 30)−1200. Calculating according to the volume percentage of the slender columns in the template, the volume percentage of the big pore channels in the porous quartz ceramics should be about 17.7%. This value is close to the open porosity (18.2%) of PQ−10−1200. As known from the pore size distribution of PQ−10−1200 measured by mercury porosimeter, the volume percentage of the small pores with mean diameter of about 10 μm is only 0.6 %, the volume percentage of the big pores with mean diameter of about 500 μm is 17.9% which is even closer to the open porosity of PQ−10−1200. According to the above results, it can be concluded with enough reason that almost all of the small pores in PQ−10−1200 are closed and independent of each other, and the highly−ordered big pore channels in PQ−10−1200 are well−connected with each other.

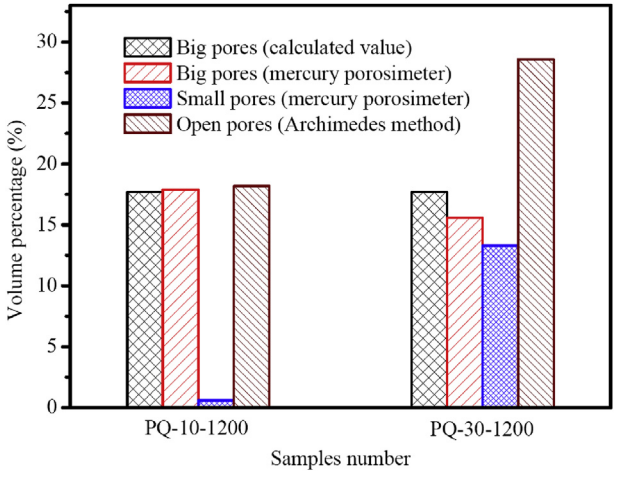

Fig. 5. Volume percentage of the pores in PQ−(10 and 30)−1200.

https://doi.org/10.1016/j.heliyon.2018.e00935

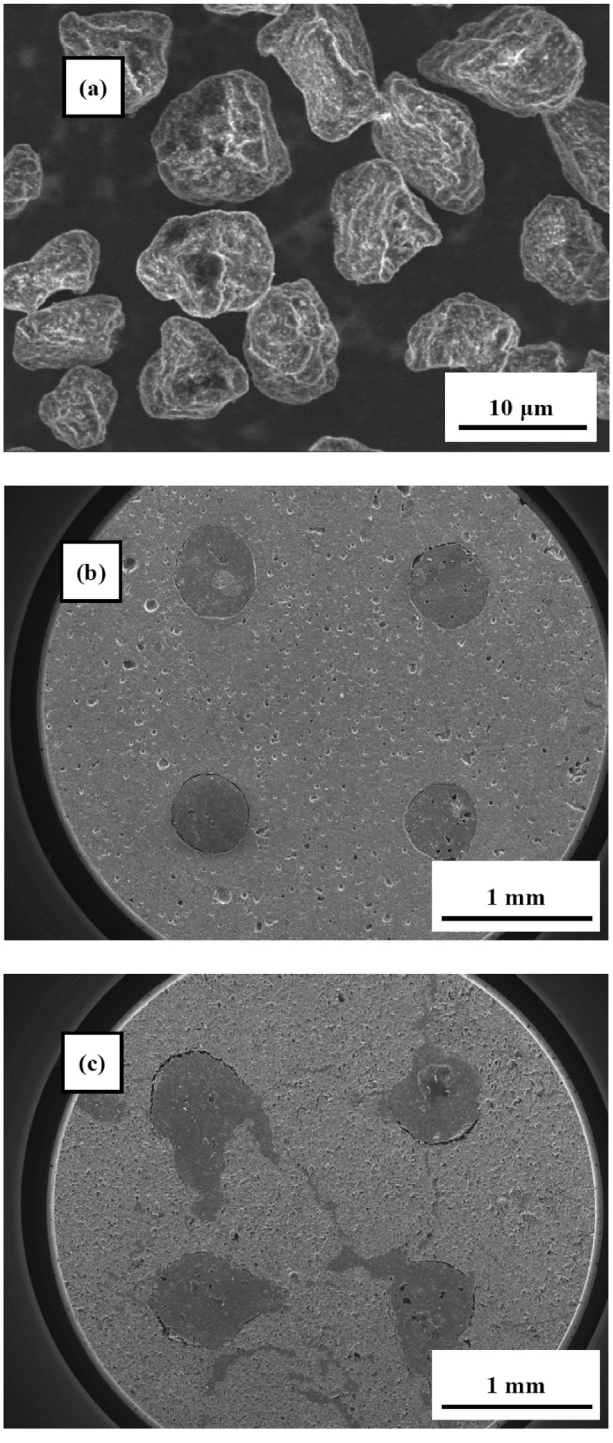

Fig. 6. SEM micrographs of (a) the carbon powder used in this work and the samples of (b) PQ−10−1200−C and (c) PQ−30−1200−C.

https://doi.org/10.1016/j.heliyon.2018.e00935

For PQ−30−1200, the open porosity (28.6%) is much higher than the calculated volume percentage of the big pore channels. From the pore size distribution measured by mercury porosimeter, the volume percentage of the small pores with mean diameter of about 30 μm is 13.3 %, and the volume percentage of the big pores with mean diameter of about 400 μm is 15.6 %. Accordingly, it can be concluded from the above results that both the large number of uniformly−distributed small pores and the highly−ordered big pore channels are well−connected with each other.

Fig. 6 shows the SEM micrographs of the carbon powder used in this work and the samples of PQ−(10 and 30)−1200−C after polishing. As shown in Fig. 6(a), the carbon grains are sphere/ellipsoid−shaped with hardly any sharp angle at surface, the diameter of the carbon grains is about 10 μm. The sphere/ellipsoid−shaped carbon grains are benefit to reducing the flow resistance of carbon powder in the big pore channels of PQ−(10 and 30)−1200−C during the impregnation process, so the big pore channels in PQ−(10 and 30)−1200−C (Fig. 6(b−c)) are fully filled with carbon powder. During the impregnation process, the carbon powder in slurry cannot enter the small pores of PQ−10−1200 because the sporadically distributed small pores in PQ−10−1200 are completely independent of each other. As shown in Fig. 6(b), there is not any carbon filler in the small pores of PQ−10−1200−C, and the cross section shape of the carbon filler in the big pore channels is perfectly round.

For PQ−30−1200, the small pores and big pore channels are well−connected with each other, so, after the big pore channels in PQ−30−1200 have been fully filled with slurry during the impregnation process, the carbon powder in slurry may have an opportunity to enter the small pores by passing through the wall of big pore channels. As can be seen from the micrograph of PQ−30−1200−C in Fig. 6(c), besides the big pore channels, some small pores especially those nearby the big pore channels are also filled with carbon powder. Due to the irregular filling of carbon powder in the small pores nearby the big pore channels, the cross section shape of the carbon filler in PQ−30−1200−C is not round but irregular.

4. Conclusions

In this study, quartz ceramics with highly−ordered and well−connected big pore channels were fabricated by a combination of 3D printing, vacuum suction filtration and sintering. The spatial lattice structure in the template together with raw material ratio and sintering temperature has great effect on the properties and pore structure of the porous quartz ceramics.

By using the PLA template printed out in this work, the porous quartz ceramics fabricated from the quartz powder with 5 wt% calcium carbonate and 5 wt% talc by sintering at 1200 °C for 2 h show sporadically distributed small pores which are

https://doi.org/10.1016/j.heliyon.2018.e00935

completely independent of each other, highly−ordered and well−connected big pore channels with diameter of about 500 μm and volume percentage of about 17.9%, open porosity of 18.2% and compression strength of 44.2 MPa.

Take the quartz ceramics with only highly−ordered and well−connected big pore channels as substrate, orderly−arranged carbon filler was successfully formed in the porous quartz ceramics by fully filling carbon powder in the big pore channels of the porous quartz ceramics via vacuum impregnation method. In the field of electromagnetic absorption, the structure of the carbon filler in quartz ceramics could easy be adjusted by changing the spatial lattice structure in the template according to the demand for electromagnetic absorbing property.

Declarations

Author contribution statement

Guojian Yuan: Conceived and designed the experiments.

Zhen Meng, Jia Guo, Guangyou Zhou: Performed the experiments.

Rui Li: Analyzed and interpreted the data.

Mengyao Zheng: Contributed reagents, materials, analysis tools or data.

Xiangming Li: Conceived and designed the experiments; Analyzed and interpreted the data; Contributed reagents, materials, analysis tools or data; Wrote the paper.

Funding statement

This work was supported by the National Natural Science Foundation of China (51479172) and Natural Science Foundation of Shandong Province (ZR2016JL020).

Competing interest statement

The authors declare no conflict of interest.

Additional information

No additional information is available for this paper.

References

[1] S. Kitaoka, Y. Matsushima, C. Chen, H. Awaji, Thermal cyclic fatigue behavior of porous ceramics for gas cleaning, J. Am. Ceram. Soc. 87 (2004) 906−913.

https://doi.org/10.1016/j.heliyon.2018.e00935

[2] P.S. Cheow, E.Z.C. Ting, M.Q. Tan, C.S. Toh, Transport and separation of proteins across platinum−coated nanoporous alumina membranes, Electrochim. Acta 53 (2008) 4669−4673.

[3] B. Naik, V.S. Prasad, N.N. Ghosh, Preparation of Ag nanoparticle loaded mesoporous γ−alumina catalyst and its catalytic activity for reduction of 4−nitrophenol, Powder Technol. 232 (2012) 1−6.

[4] J. Newnham, K. Mantri, M.H. Amin, J. Tardio, S.K. Bhargava, Highly stable and active Ni−mesoporous alumina catalysts for dry reforming of methane, Int. J. Hydrogen Energy 37 (2012) 1454−1464.

[5] B. H Yoon, Y.H. Koh, C.S. Park, H.E. Kim, Generation of large pore channels for bone tissue engineering using camphene−based freeze casting, J. Am. Ceram. Soc. 90 (2007) 1744−1752.

[6] B.H. Yoon, W.Y. Choi, H.E. Kim, J.H. Kim, Y.H. Koh, Aligned porous alumina ceramics with high compressive strengths for bone tissue engineering, Scripta Mater. 58 (2008) 537−540.

[7] S.Q. Ding, Y.P. Zeng, D.L. Jiang, Oxidation bonding of porous silicon nitride ceramics with high strength and low dielectric constant, Mater. Lett. 61 (2007) 2277−2280.

[8] X.M. Li, X.W. Yin, L.T. Zhang, L.F. Cheng, Y.C. Qi, Mechanical and dielectric properties of porous Si_3N_4−SiO_2 composite ceramics, Mater. Sci. Eng. A 500 (2009) 63−69.

[9] S. Janbuala, M. Eambua, A. Satayavibul, W. Nethan, Effect of bagasse and bagasse ash levels on properties of pottery products, Heliyon 4 (2018), e00814, 1−12.

[10] X.M. Li, L.T. Zhang, X.W. Yin, Microstructure and mechanical properties of three porous Si3N4 ceramics fabricated by different techniques, Mater. Sci. Eng. A 549 (2012) 43−49.

[11] M. Kitiwan, D. Atong, Effects of porous alumina support and plating time on electroless plating of palladium membrane, J. Mater. Sci. Technol. 26 (2010) 1148−1152.

[12] M. Potoczek, Gelcasting of alumina foams using agarose solutions, Ceram. Int. 34 (2008) 661−667.

[13] M. Takahashi, R.L. Menchavez, M. Fuji, H. Takegami, Opportunities of porous ceramics fabricated by gelcasting in mitigating environmental issues, J. Eur. Ceram. Soc. 29 (2009) 823−828.

 https://doi.org/10.1016/j.heliyon.2018.e00935

[14] C.R. Zou, C.R. Zhang, B. Li, S.Q. Wang, F. Cao, Microstructure and properties of porous silicon nitride ceramics prepared by gel−casting and gas pressure sintering, Mater. Des. 44 (2013) 114−118.

[15] Y.M. Zhang, L.Y. Hu, J.C. Han, Z.H. Jiang, Freeze casting of aqueous alumina slurries with glycerol for porous ceramics, Ceram. Int. 36 (2010) 617−621.

[16] Y.F. Xia, Y.P. Zeng, D.L. Jiang, Microstructure and mechanical properties of porous Si_3N_4 ceramics prepared by freeze−casting, Mater. Des. 33 (2012) 98−103.

[17] R.B. Zhang, D.N. Fang, X.M. Chen, Y.M. Pei, Z.D. Wang, Y.S. Wang, Microstructure and properties of highly porous Y_2SiO_5 ceramics produced by a new water−based freeze casting, Mater. Des. 46 (2013) 746−750.

[18] D. Zhang, C. Meggs, T.W.P. Button, Porous Al_2O_3−ZrO_2 composites fabricated by an ice template method, Scripta Mater. 62 (2010) 466−468.

[19] X. He, X.G. Zhou, B. Su, 3D interconnective porous alumina ceramics via direct protein foaming, Mater. Lett. 63 (2009) 830−832.

[20] K. Takagi, T. Takahashi, K. Kikuchi, A. Kawasaki, Fabrication of bioceramic scaffolds with ordered pore structure by inverse replication of assembled particles, J. Eur. Ceram. Soc. 30 (2010) 2049−2055.

[21] J.G. Dellinger, J.A.C. Eurell, R.D. Jamison, Bone response to 3D periodic hydroxyapatite scaffolds with and without tailored microporosity to deliver bone morphogentic protein 2, J. Biomed. Mater. Res. 76A (2006) 366−376.

[22] K.A. Hing, B. Annaz, S. Saeed, P.A. Revell, T. Buckland, Microporosity enhances bioactivity of synthetic bone graft substitutes, J. Mater. Sci. Mater. Med. 16 (2005) 467−475.

[23] J.R. Woodard, A.J. Hilldore, S.K. Lan, C.J. Park, A.W. Morgan, J.A.C. Eurell, S.G. Clark, M.B. Wheeler, R.D. Jamison, A.J.W. Johnson, The mechanical properties and osteoconductivity of hydroxyapatite bone scaffolds with multi−scale porosity, Biomaterials 28 (2007) 45−54.

[24] N.Q. Zhao, T.C. Zou, C.S. Shi, J.J. Li, W.K. Guo, Microwave absorbing properties of activated carbon−fiber felt screens (vertical−arranged carbon fibers)/epoxy resin composites, Mater. Sci. Eng. B 127 (2006) 207−211.

[25] T.C. Zou, C.S. Shi, N.Q. Zhao, Microwave absorbing properties of activated carbon−fiber felt dipole array/epoxy composites, J. Mater. Sci. 42 (2007) 4870−4876.

https://doi.org/10.1016/j.heliyon.2018.e00935

[26] D.C. Jia, Y. Zhou, T.Q. Lei, Ambient and elevated temperature mechanical properties of hot−pressed fused silica matrix composite, J. Eur. Ceram. Soc. 23 (2003) 801−808.

[27] J.S. Lyons, T.L. Starr, Strength and toughness of slip−cast fused silica composites, J. Am. Ceram. Soc. 77 (1994) 1673−1675.

[28] D. Njoya, A. Elimbi, D. Fouejio, M. Hajjaji, Effects of two mixtures of kaolin−talc−bauxite and firing temperatures on the characteristics of cordierite−based ceramics, J. Build. Eng. 8 (2016) 99−106.

[29] H.R. Baharvandi, A.M. Hadian, H. Abdizade, N. Ehsani, Investigation on addition of talc on sintering behavior and mechanical properties of B_4C, J. Mater. Eng. Perform. 15 (2006) 280−283.

[30] F.L. Yu, J.F. Yang, Y.H. Xue, J. Du, Y. Lu, J.Q. Gao, Effects of talc and clay addition on pressureless sintering of porous Si_3N_4 ceramics, Bull. Mater. Sci. 32 (2009) 177−181.

 https://doi.org/10.1016/j.heliyon.2018.e00935